Surface & Coatings Technology 231 (2013) 176–179

Contents lists available at ScienceDirect

Surface & Coatings Technology

journal homepage: www.elsevier.com/locate/surfcoat

Rapid thermal annealing effects on the structural and nanomechanical properties of Ga-doped ZnO thin films

S.-R. Jian [a,*], G.-J. Chen [a], S.-K. Wang [a], T.-C. Lin [a], J.S.-C. Jang [b,c], J.-Y. Juang [d], Y.-S. Lai [e], J.-Y. Tseng [f]

[a] Department of Materials Science and Engineering, I-Shou University, Kaohsiung 840, Taiwan
[b] Institute of Materials Science and Engineering, National Central University, Chung-Li 320, Taiwan
[c] Department of Mechanical Engineering, National Central University, Chung-Li 320, Taiwan
[d] Department of Electrophysics, National Chiao Tung University, Hsinchu 300, Taiwan
[e] Central Product Solutions, Advanced Semiconductor Engineering, Nantze Export Processing Zone, Kaohsiung 811, Taiwan
[f] Institute of Physics, Academia Sinica, Taipei 11529, Taiwan

ARTICLE INFO

Available online 27 June 2012

Keywords:
Ga-doped ZnO thin films
XRD
AFM
Nanoindentation
Hardness

ABSTRACT

In this study, the structural and nanomechanical properties of Ga-doped ZnO (GZO) thin films on glass substrates followed by rapid thermal annealing (RTA) process were investigated by X-ray diffraction (XRD), atomic force microscopy (AFM) and nanoindentation techniques. The XRD results indicated that the annealed GZO thin films are textured, having a preferential crystallographic orientation along the hexagonal wurtzite (002) axis. Both the grain size and surface roughness of the annealed GZO thin films exhibit an increasing trend after RTA treatment. The hardness and Young's modulus of the annealed GZO thin films were measured by a Berkovich nanoindenter operated with the continuous contact stiffness measurements (CSM) option. Furthermore, the hardness and Young's modulus were found to increase with increasing grain size when the RTA time was prolonged from 0.5 to 3 min. The deformation behavior is referred to the inverse Hall–Petch effect commonly observed in systems deformed primarily via grain boundary sliding. The suppression of dislocation movement-associated deformation mechanism might be arisen from strong pinning effects introduced by Ga-doping.

© 2012 Elsevier B.V. All rights reserved.

1. Introduction

ZnO has been considered a material of high potential in optoelectronics and spintronics applications [1–3]. Although recently doping ZnO into *p*-type has been the subject that has attracted much more attention in ZnO researches, the *n*-type materials with high quality crystallinity and controllable electron carrier concentration are also indispensable toward the applications. For example, being able to control the electron carrier concentration is important for making the ZnO-based dilute magnetic semiconductors because their magnetic properties can be thereby modulated [4]. Moreover, group-III-doped ZnO with large electron carrier concentration is a potential candidate for replacing conventional transparent conducting oxides such as indium tin oxide. Among group-III element, Ga is an excellent *n*-type dopant for ZnO owing to the more compatible covalent bond length between Ga-O and ZnO (1.92 Å for Ga-O and 1.97 Å for Zn-O) than that of Al-O (2.7 Å)and In-O (2.1 Å).

Ga-doped ZnO (GZO) thin films have been widely investigated and used in optoelectronic as well as electronic devices [5,6]. However, their mechanical properties are largely ignored. Since for most device fabrication processes contact-induced damage may significantly affect the ultimate optical and electronic properties of the device, thus a quantitative assessment of the material's mechanical properties is of crucial importance. Nanoindentation has been widely used for charactering the mechanical properties of solid surface and thin films [7,8]. Among the mechanical properties of interest, hardness, Young's modulus, elastic/plastic deformation behavior can be obtained from nanoindentation testing [9–11].

It is well known that the properties of ZnO thin films are strongly affected not only by the deposition conditions [12,13] but also by the post-annealing conditions [14]. Post-annealing has a large effect on the crystallinity of ZnO thin films, such as grain size, residual strain and so on, thus, it is also an important method for manipulating the mechanical characteristics of the materials [15]. In this study, we aimed to investigate the nanomechanical properties of GZO thin films by means of nanoindentation. The GZO films were deposited on glass substrates using a radio frequency (rf) magnetron sputtering system. The film microstructures were characterized by X-ray diffraction (XRD) and the surface morphology was examined by atomic force microscopy (AFM). Furthermore, the influences of the rapid thermal annealing (RTA) on the properties of the GZO thin films are also presented.

* Corresponding author. Tel.: +886 7 6577711x3130; fax: +886 7 6578444.
E-mail address: srjian@gmail.com (S.-R. Jian).

0257-8972/$ – see front matter © 2012 Elsevier B.V. All rights reserved.
doi:10.1016/j.surfcoat.2012.06.060

2. Experimental details

Experimentally, the 3 at% Ga-doped ZnO (GZO) thin films were deposited on Corning 1737 F glass substrates at room temperature by using rf-magnetron sputtering. The detailed growth procedures and operation parameters can be found elsewhere [16]. Subsequently, the as-deposited GZO thin films were post-annealed at 500 °C for 0.5, 1, 2 and 3 min in oxygen environment by rapid thermal annealing (RTA). During the annealing process, the rising or cooling rate of the temperature was kept at 30 °C/s.

The crystal structure of GZO thin films were analyzed by X-ray diffraction (Panalytical X'Pert XRD, CuKα, λ = 1.5406 Å). The Scherrer's formula shown below was employed to estimate the mean grain size of GZO thin films [17]:

$$D = \frac{0.9\lambda}{B\cos\theta} \tag{1}$$

Hereλ, B and θ denote the X-ray wavelength, the FWHM of (002) peak, and the corresponding Bragg diffraction angle, respectively.

In addition, the examinations of surface features were carried out by using AFM (Topometrix-Accures-II). The average surface roughness, R_{RMS} of the surface was calculated by the following equation [18]:

$$R_{RMS} = \sqrt{\frac{1}{N}\sum_{n=1}^{N} r_n^2} \tag{2}$$

Here N is the number of data and r_n is the surface height of the nth datum.

Nanoindentation experiments were preformed on a MTS Nano Indenter® XP system with a three-sided pyramidal Berkovich indenter tip by using the continuous stiffness measurement (CSM) technique [19]. This technique is accomplished by imposing a small, sinusoidal varying force on top of the applied linear force that drives the motion of the indenter. The displacement response of the indenter at the excitation frequency and the phase angle between the force and displacement were measured continuously as a function of the penetration depth. Solving for the in-phase and out-of-phase portions of the displacement response gives rise to the determination of the contact stiffness as a continuous function of depth [19]. As such, the mechanical properties changing with respect to the indentation depth can be obtained. The nanoindentation measurements were carried out as follows. First, prior to applying loading on ZnO sample, nanoindentation was conducted on a standard fused silica sample to obtain the reasonable range (the Young's modulus of fused silica is 68 ~ 72 GPa). Then, a constant strain rate of 0.05 s^{-1} was maintained during the increment of load until the indenter reached a depth of 100 nm into the surface. The load was then held at the maximum value of loading for 10 s in order to avoid the creep which might significantly affect the unloading behavior. The indenter was then withdrawn from the surface at the same rate until the loading has reduced to 10% of the maximum load. Then, the indenter was completely removed from the material. In this work, constant strain rate was chosen in order to minimize the strain-hardening effects. At least 20 indentations were performed on each sample and the distance between the adjacent indents was kept at least 50 μm apart to avoid interaction.

The hardness, H, and elastic modulus, E, were calculated from the load–displacement data following the work reported by Oliver and Pharr [20].

$$H = \frac{P_{\max}}{A_p} \tag{3}$$

where $P_{\max}$ is the load measured at a maximum penetration depth (h) and A_p is the projected contact area between the indenter and the sample at $P_{\max}$.

The reduced elastic modulus (E_r), which is the combined elastic modulus of both the tested sample and the indenter, is calculated as follows:

$$E_r = \frac{\sqrt{\pi}}{2}\frac{S}{\sqrt{A_p}} \tag{4}$$

where $S = dP/dh$ (stiffness) is the slope of the upper portion of the unloading curve in the load–displacement curve.

The elastic modulus of thin films, E_f, is then calculated as follows:

$$E_f = \left(1-v_f^2\right)\left(\frac{1}{E_r} - \frac{1-v_i^2}{E_i}\right)^{-1} \tag{5}$$

Here v is the Poisson's ratio and the subscripts i and f denote the parameters for the indenter and the annealed ZnO thin films, respectively. For diamond indenter tip, $E_i = 1141$ GPa, $v_i = 0.07$ and, $v_f = 0.25$ are chosen for ZnO sample [21].

3. Results and discussion

Fig. 1 presents the XRD patterns of GZO thin films with RTA time varying from 0.5 to 3 min. It can be found that the preferred orientation of the films has been modified with the variation of RTA time durations. With the increase in the RTA time, peak intensities are seen to increase. Note that there is no evidence of the existence of Ga_2O_3 phase discernible from the XRD results, implying that Ga atoms either have completely substituted for Zn atoms in the ZnO lattice or they might segregate into the amorphous regions in the vicinity of grain boundaries. In addition, an intense (101) peak is observed in all of the annealed GZO films, indicating that the films were largely growing with the (101) plane parallel to the surface of the substrate. On the other hand, (002) is commonly regarded as the preferred orientation for films with hexagonal wurtzite structure, because thermodynamically the (001) plane has a lower surface energy than all the other planes in this particular structure. Therefore, increasing the RTA time properly may favor the atoms to diffuse to the equilibrium positions, hence the preferred orientation becomes more of the (002) characteristic and the film crystallinity was improved significantly at the same time. The mean grain sizes of GZO thin films were estimated to be 38.4, 42.3, 44.2 and 45.8 nm (compared with 23.5 nm for as-deposited GZO film) for films respectively annealed at RTA time of 0.5, 1, 2 and 3 min.

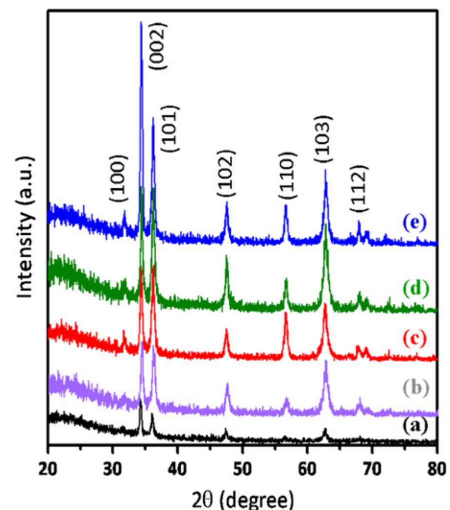

Fig. 1. XRD patterns of (a) as-deposited GZO thin film, and GZO thin films annealed at different RTA time durations: (b) 0.5 min, (c) 1 min, (d) 2 min, and (e) 3 min.

Fig. 2 illustrates the surface morphologies of the annealed GZO thin films obtained by AFM. It is evident that, as the RTA time increases from 0.5 to 3 min, the average surface roughness is increased from 7.2 to 9.3 nm. It is because the longer RTA time provides more activation energy to stimulate the migration of grain boundaries and coalescence of adjacent grains, leading to larger grains and rougher surface [15,22]. Therefore, it can be observed that fewer grain boundaries and larger grains are evidently displayed in films with longer RTA time.

The effects of RTA on the mechanical performance of GZO thin films were evaluated directly by using nanoindentation measurements. The typical load–displacement curves for the as-deposited and annealed GZO thin films are plotted in Fig. 3. The load–displacement responses obtained by nanoindentation contain information about the elastic and plastic deformation behaviors and can be regarded as the "fingerprints" of the film's mechanical properties. It is evident that, for the RTA-treated films, both the film hardness and the elasticity recovery are significantly enhanced, as compared to the as-deposited ones. The hardness and Young's modulus of as-deposited and annealed GZO thin films, extracted from the load–displacement curves as a function of penetration depth, are displayed in Fig. 4(a)–(b). As a function of the penetration depth, both the hardness and Young's modulus reach a maximum value and then start to decrease until finally reaching a constant value. Comparing the hardness curve of annealed GZO thin films with that of the as-deposited films, an enhancement of the hardness from 8.5 to 10.8 GPa was observed, while the Young's modulus is enhanced from 120 to 155 GPa when the indenter penetration depth is greater than 30 nm. The effects of RTA time variation on the hardness and Young's modulus of the annealed GZO thin films are summarized in Table 1. Furthermore, Wang and Li [23] proposed a similar size dependence of elastic modulus for ZnO nanowires. Because of the influences of surface stress effect, while the diameter size is larger than 20 nm, the Young's modulus increases with the diameter size. Similar

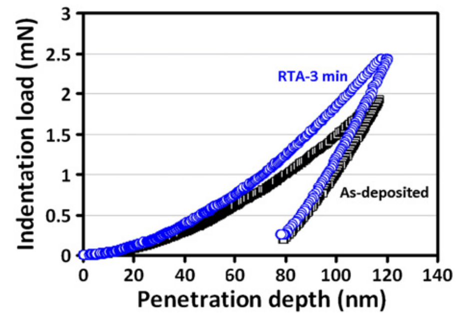

Fig. 3. Typical load–displacement curve for the as-deposited and annealed GZO thin films.

size effect might work in the GZO thin films. In overall, the values of Young's modulus of GZO thin films are lower than those of the bulk GZO, which is consistent with the previous studies [24,25].

Also shown in Table 1 are the ratios H/E_f and H^3/E_f^2 for all GZO samples. The H/E_f value characterizes the susceptibility of materials to the elastic strain. Therefore, increasing the H/E_f value can be translated into a correspondent enhancement in the wear resistance [26]. On the other hand, the parameter, H^3/E_f^2, describes the ability of a material in resisting against the plastic deformation and, thus, characterizes its toughness and resistance to crack propagations [27]. The larger values of H/E_f and H^3/E_f^2 often represent as a reliable indicator of good wear resistance. The current results indicated that GZO films subjected to 3 min-RTA treatment exhibited the best combinations in terms of the primary mechanical property parameters examined.

According to the above-mentioned results, it is evident that the primary effects of RTA, represented mainly by the duration of the RTA time here, were to increase the grain size of GZO films, which

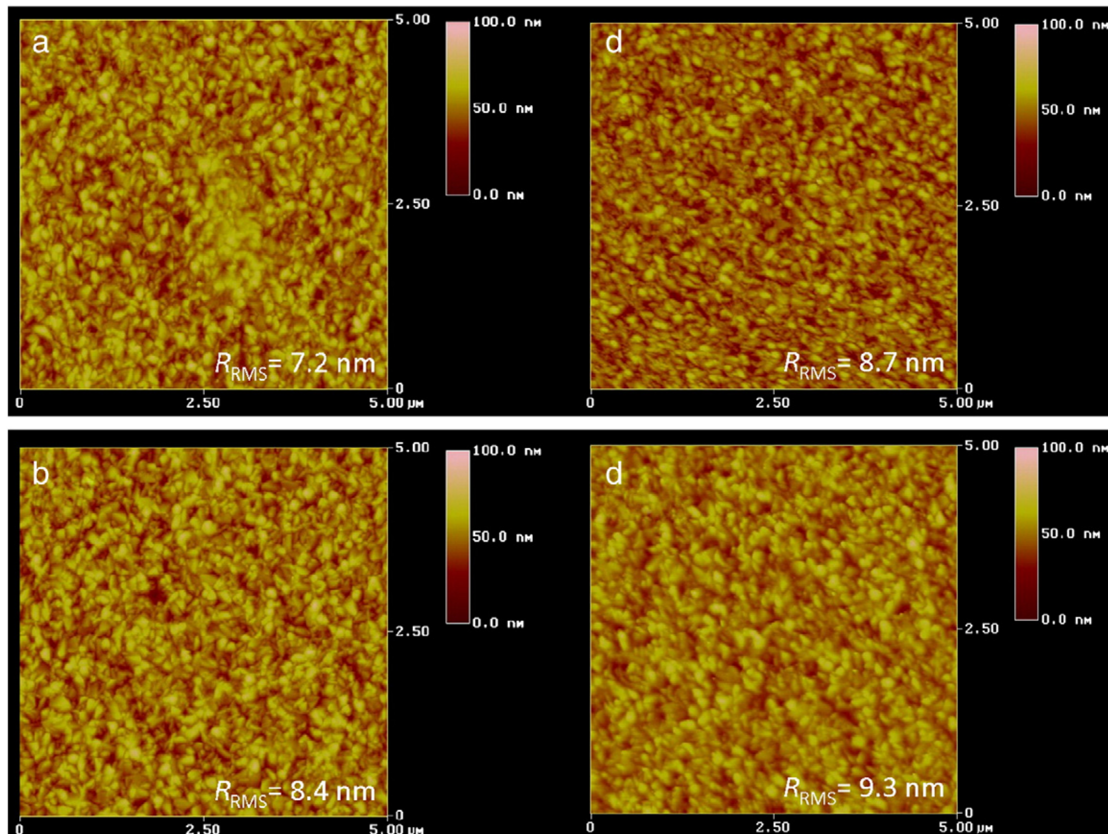

Fig. 2. AFM images of annealed GZO thin films at the different RTA time durations: (a) 0.5 min, (b) 1 min, (c) 2 min, and (d) 3 min.

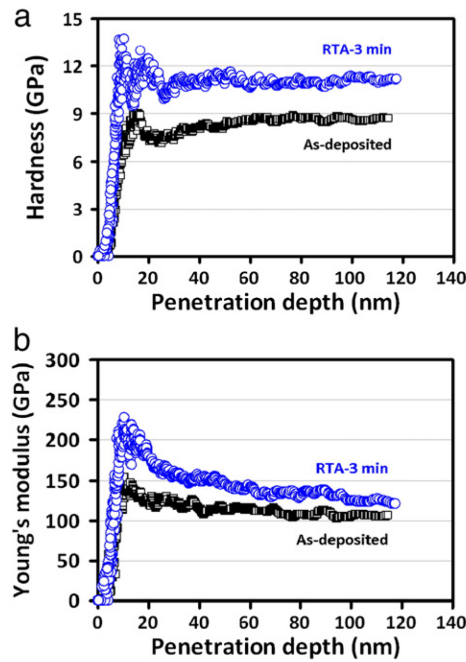

Fig. 4. (a) Hardness and (b) Young's modulus as a function of the penetration depth for as-deposited and annealed GZO thin films.

in turn led to significant enhancements in various aspects of the film's mechanical properties. Since the variation of hardness with the grain size appears to follow the inverse Hall–Petch effect [28], that is the hardness increases with grain size, it is suggestive that the most prominent deformation mechanism prevailing in the current GZO films could be arisen from grain boundary sliding instead of from dislocation movements. We believe that the doping of Ga may have induced significant dislocation pinning effects, which in turn hindered the dislocation activities and activated the secondary deformation mechanism as an alternative. It should be interesting to carry out further prolonged RTA treatments to see what will happen when the film grain size is further increased.

4. Conclusion

A combination of XRD, AFM and nanoindentation techniques has been carried out to investigate the structural, surface morphological features, and nanomechanical properties of GZO films subjected to RTA treatment with various time durations. The XRD results indicated that the annealed GZO thin films had the hexagonal wurtzite structure with a predominant (002) growth orientation. Prolonged RTA duration appeared to facilitate the grain growth, leading to increased film surface roughness, as evident from AFM observations. The hardness and Young's modulus of GZO films were respectively ranging from 7.8 to 10.8 GPa and from 105.4 to 130.6 GPa when the RTA time was increased from 0.5 to 3 min. The fact that the hardness of the GZO films behaves in accordance with the inverse Hall–Petch effect indicates that Ga doping might have changed the prevailing deformation mechanism from dislocation movement for pristine ZnO to grain boundary sliding by introducing substantial pinning effects.

Table 1
The data evaluated from XRD patterns, AFM images and nanoindentation results of measured GZO thin films in this study.

GZO	D (nm)	R_{RMS} (nm)	H (GPa)	E_f (GPa)	H/E_f	H^3/E_f^2
As-deposited	23.5	5.5	8.5	113.4	0.075	0.047
RTA-0.5 min	38.4	7.2	7.8	105.4	0.074	0.043
RTA-1 min	42.3	8.4	9.5	115.2	0.081	0.064
RTA-2 min	44.2	8.7	10.2	126.8	0.080	0.066
RTA-3 min	45.8	9.3	10.8	130.6	0.083	0.074

Acknowledgements

This work was partially supported by the National Science Council of Taiwan, under Grant No.: NSC100-2221-E-214-024. JYJ is partially supported by the NSC of Taiwan and the MOE-ATU program operated at NCTU. The author likes to thank Dr. P.-F. Yang and Dr. Y.-T. Chen for their technical supports.

References

[1] T. Aoki, Y. Hatanaka, D.C. Look, Appl. Phys. Lett. 76 (2000) 3257.
[2] C. Klingshim, Phys. Status Solidi B 244 (2007) 3027.
[3] F. Pan, C. Song, X.J. Liu, Y.C. Yang, F. Zeng, Mater. Sci. Eng., R 62 (2008) 1.
[4] Z. Yang, J.L. Liu, M. Biasini, W.P. Beyermann, Appl. Phys. Lett. 92 (2008) 042111.
[5] H. Makino, T. Yamada, N. Yamamoto, T. Yamamoto, Thin Solid Films 519 (2010) 1521.
[6] Y.Y. Liu, S.Y. Yang, G.X. Wei, H.S. Song, C.F. Cheng, C.S. Xue, Y.Z. Yuan, Surf. Coat. Technol. 205 (2011) 3530.
[7] S.R. Jian, J.S.C. Jang, Y.S. Lai, P.F. Yang, C.S. Yang, H.C. Wen, C.H. Tsai, Mater. Chem. Phys. 109 (2008) 360.
[8] S.R. Jian, H.G. Chen, G.J. Chen, J.S.C. Jang, J.Y. Juang, Curr. Appl. Phys. 12 (2012) 849.
[9] S.R. Jian, G.J. Chen, T.C. Lin, Nanoscale Res. Lett. 5 (2010) 935.
[10] S.R. Jian, J.Y. Juang, N.C. Chen, J.S.C. Jang, J.C. Huang, Y.S. Lai, Nanosci. Nanotechnol. Lett. 2 (2010) 315.
[11] S.R. Jian, J.Y. Juang, J. Nanomater. 2012 (2012) 914184.
[12] P.F. Yang, H.C. Wen, S.R. Jian, Y.S. Lai, S. Wu, R.S. Chen, Microelectron. Reliab. 48 (2008) 389.
[13] H. Chen, J. Ding, S. Ma, Phys. E 42 (2010) 1487.
[14] J.H. Han, Y.S. No, T.W. Kim, J.Y. Lee, J.Y. Kim, W.K. Choi, Appl. Surf. Sci. 256 (2010) 1920.
[15] L.Y. Lin, D.E. Kim, Thin Solid Films 517 (2009) 1690.
[16] J.Y. Tseng, Y.T. Chen, M.Y. Yang, C.Y. Wang, P.C. Li, W.C. Yu, Y.F. Hsu, S.F. Wang, Thin Solid Films 517 (2009) 6310.
[17] B.D. Cullity, S.R. Stock, In: Element of X-ray Diffraction, Prentice Hall, New Jersey, 2001, p. 170.
[18] K. Miyoshi, Y.W. Chung, Surface Diagnostics in Tribology: Fundamental Principles and Applications, World Scientific Publishing, Singapore, 1993..
[19] X.D. Li, B. Bhushan, Mater. Charact. 48 (2002) 11.
[20] W.C. Oliver, G.M. Pharr, J. Mater. Res. 7 (1992) 1564.
[21] C.Y. Yen, S.R. Jian, G.J. Chen, C.M. Lin, H.Y. Lee, W.C. Ke, Y.Y. Liao, P.F. Yang, C.T. Wang, Y.S. Lai, J.S.C. Jang, J.Y. Juang, Appl. Surf. Sci. 257 (2011) 7900.
[22] Y. Lin, J. Xie, H. Wang, Y. Li, C. Chavez, S. Lee, S.R. Foltyn, S.A. Crooker, A.K. Burrell, T.M. McCleskey, Q.X. Jia, Thin Solid Films 101 (2005) 492.
[23] G.F. Wang, X.D. Li, Appl. Phys. Lett. 91 (2007) 231912.
[24] X.Y. Tao, X.N. Wang, X.D. Li, Nano Lett. 7 (2007) 3172.
[25] H. Ni, X.D. Li, Nanotechnology 17 (2006) 3591.
[26] A. Leyland, A. Mattews, Wear 246 (2000) 1.
[27] D. Galvan, Y.T. Pei, J.T.M. De Hosson, Surf. Coat. Technol. 200 (2006) 6718.
[28] J. Schiotz, T. Vegge, F.D. Di Tolla, K.W. Jacobsen, Phys. Rev. B 60 (1999) 11971.